Analysis and Quantification of a Solid-State Laser Doppler Anemometer

C. McLean* and C. Camci†

Pennsylvania State University, University Park, Pennsylvania 16802

A single component, visible wavelength, heterodyne laser Doppler anemometer was constructed based on solid-state laser diode technology for use in fluid dynamic research. With the recent advancements in solid-state laser diodes and solid-state avalanche photodiodes, it is possible to construct miniature laser Doppler anemometer systems solely employing solid-state technology. Such systems have the advantages of small size, light weight, low-power consumption, low cost, and ruggedness. The subject of the current research was to quantitatively evaluate a miniaturized laser Doppler anemometer system constructed with visible laser diodes and an avalanche photodiode detector. Evaluation measurements in a turbulent, stagnating jet are presented and compared to both hot-wire and five-hole probe data. The miniature solid-state laser Doppler anemometer system was found to agree within 2% for mean velocities and agree within 5–20% for root mean square turbulent velocities.

Nomenclature

B	= bias error
D	= beam dimension of focused laser beam near the focal point, or stagnation jet exit diameter
d_0	= beam dimension of prefocused laser beam
E	= electric field magnitude
e	= natural exponential function, 2.7182818...
F_D	= Doppler frequency
f	= front lens focal length
H	= distance from jet exit plane to stagnation plate
h	= probe volume height
I	= intensity of the electric field, in general, E^2
l	= probe volume length
N	= number of measurements
P	= parameter, variable in equation
Re	= Reynolds number based on the mean velocity
r	= result via an equation
S	= precision index
t	= student t value, statistical quantity
u	= velocity
w	= probe volume width
X_i	= individual measurement
x, y, z	= global coordinates
x', z'	= local coordinates attached to beam A or B
ΔI	= fringe height, or fringe visibility
θ	= laser beam crossing angle
λ	= laser diode mean wavelength
ξ	= Lorentzian distribution constant, 0.145494...

Subscripts

A, B	= beam A or B, respectively
rms	= root mean squared value
r	= result
x, y, z	= in the x, y, or z direction, respectively

I. Introduction

THIS study deals with the quantitative fluid dynamic evaluation of a single component, heterodyne, laser diode-based

laser Doppler anemometer (LDA). After evaluating prior studies, it was noted that many laser diode-based LDA systems had been constructed.[1-4] However, no extensive fluid dynamic evaluation of such a system had been performed. Previous studies were concerned with proof of concept rather then the development of an accurate measurement tool. It was decided that a detailed evaluation of a laser diode LDA system would be very beneficial in determining the usefulness and future of laser diode-based LDA for fluid dynamic measurements. Essentially, could a laser diode be used to generate accurate LDA mean and turbulence quantities in a real fluid flow? The end result of the design and evaluation process was to develop an LDA system with the high accuracies necessary for fluid dynamic research.

A typical laser diode beam is characterized with many traits which make its use in LDA systems questionable.[5] However, with proper optical correction techniques, solid-state lasers can be successfully used in LDA systems. A schematic of an index guided laser diode is shown in Fig. 1. A suitable visible laser diode was found which had the qualities necessary for use in a heterodyne LDA. The visible laser diode was combined with essential optical components (collimator, circularizer, beam splitter, lenses, mirror, pinhole, and avalanche photodiode) to form the miniature laser diode-based LDA. The specifications of the miniature system are given in Table 1, and a schematic of the complete LDA system is shown in Fig. 2.
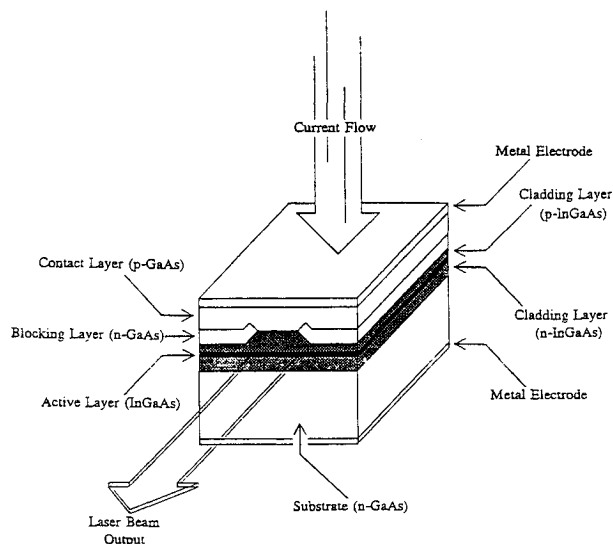
*Graduate Research Assistant, Department of Aerospace Engineering, Turbomachinery Heat Transfer Laboratory; currently at Techkor Instrumentation, State College, PA 16801. Member AIAA.

†Associate Professor, Department of Aerospace Engineering, Turbomachinery Heat Transfer Laboratory. Member AIAA.

Fig. 1 Index guided laser diode.

Table 1   Miniature solid-state LDA attributes prior to corrective measures

Specification	Quantity
Diode manufacturer	Toshiba
Diode style, mw, nm	10,670 visible red, index guided
Diode astigmatism, μm	11
Diode polarization ratio	400:1
Diode lasing mode	Single spatial and temporal
Diode temperature drift, nm/°C	0.25, including mode hoping effects
Diode beam divergence, deg	$\sim 11 \times \sim 40$ in far field
Diode intensity profile	Lorentzian/Gaussian in perpendicular and parallel transverse directions, respectively
Beam shape	Elliptical (4–1) in far field
Overall LDA size, mm	250 length,100 diameter
Main objective focal length, mm	150–300
Half-angle $\theta/2$, deg	9.939 at 150-mm focal length
Fring separation, μm	1.94 at 150-mm focal length
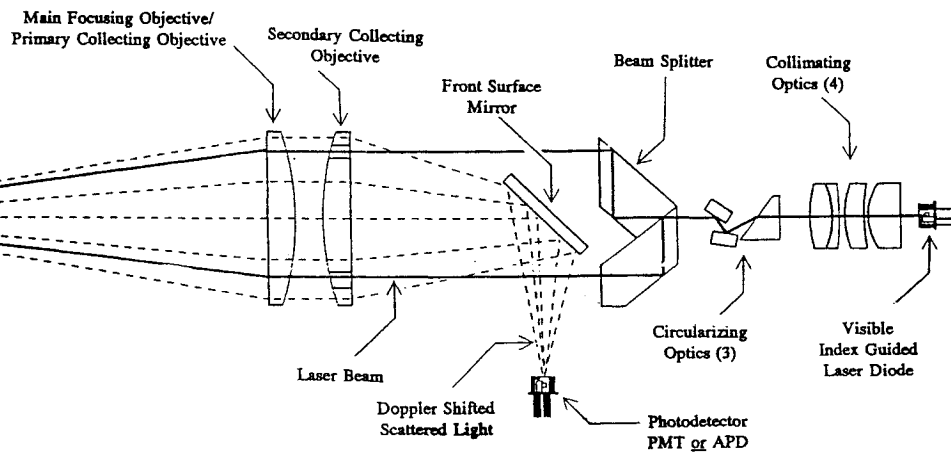
Fig. 2   Schematic of the miniature LDA system, not to scale.
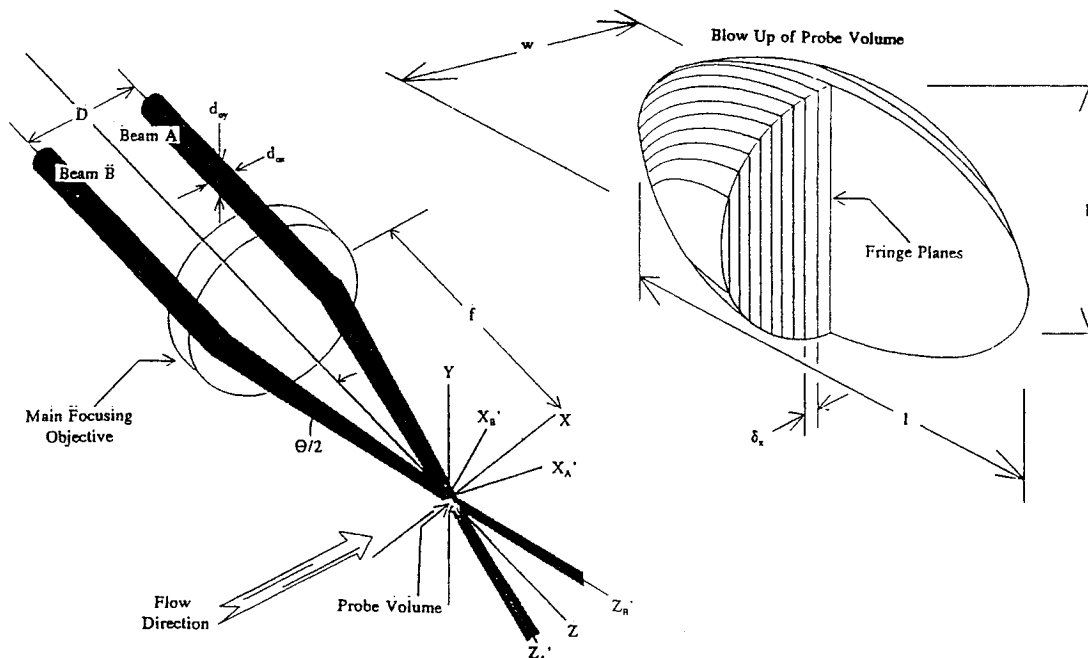
Fig. 3   Heterodyne LDA system with enlarged probe volume.

The use of a solid-state laser allows the miniaturization of LDA transmission systems, but with the expectation of degraded performance due to poor beam characteristics. Crucial areas that required consideration were low-power, high divergence, high astigmatism, elliptical beam, non-Gaussian intensity profile, coherence length, and wavelength drift. Only with a properly selected laser diode and following multiple correctional measures could an accurate LDA system be achieved.

II.   Laser Diode Probe Volume Quantification

There are substantial differences between a standard LDA probe volume based on a circular, Gaussian laser and one based on an elliptical, non-Gaussian diode laser. Figure 3 shows a standard heterodyne LDA system with enlarged probe volume (ellipsoid). It has been shown by Bopp et al.[1] that for a collimated laser diode the normalized transverse optical field magnitudes may be adequately
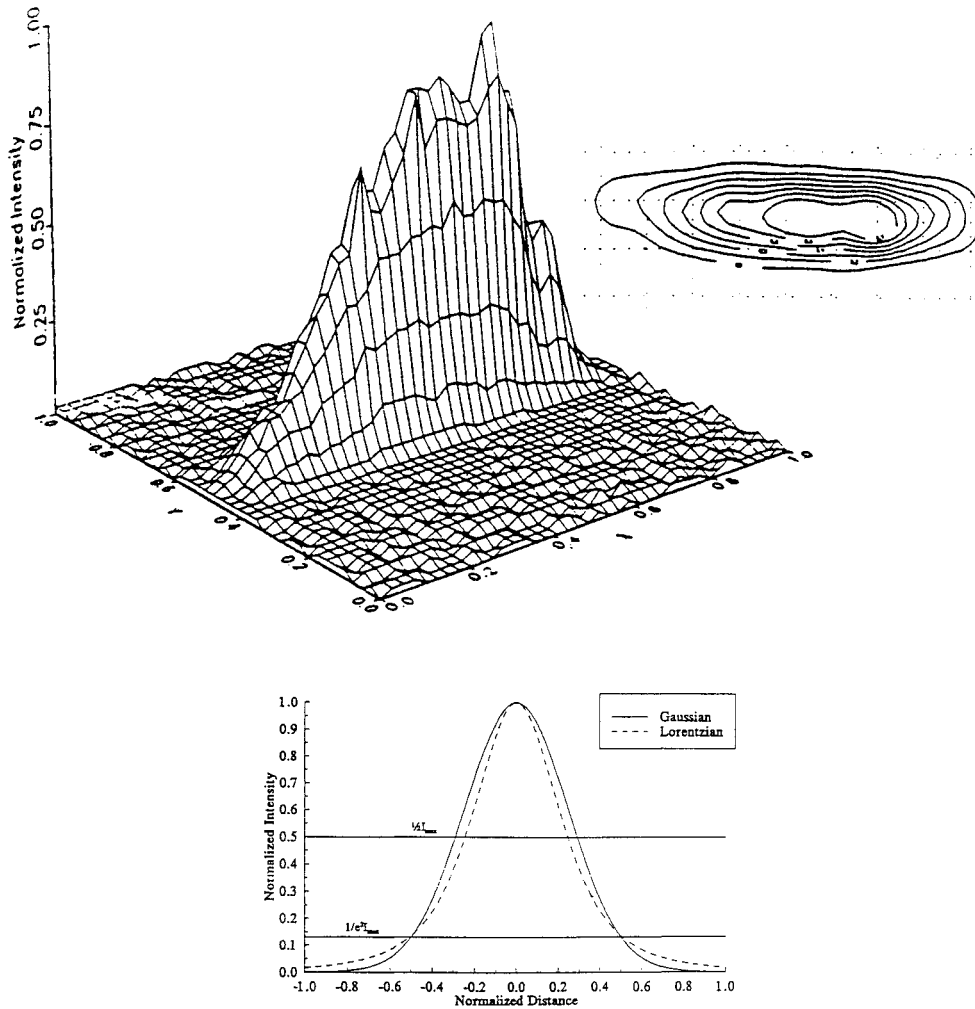
Fig. 4   Elliptical intensity profile of laser diode and a comparison of Lorentzian and Gaussian profiles.

represented by Eqs. (1) and (2) (Gaussian and Lorentzian distributions, respectively):

$$E_y = e^{-(2y/D_y)^2} \tag{1}$$

$$E_x = \xi D_x^2 / \left(\xi D_x^2 + x^2 \right) \tag{2}$$

Where ξ is given by

$$\xi = 1/[4(e-1)] \approx 0.1454941 \tag{3}$$

The electrical field distribution in the parallel transverse direction is given by E_x whereas the perpendicular transverse field distribution is given by E_y. Not only do the field distributions differ in the two transverse directions, but the beam dimensions typically differ as well. Figure 4 displays the measured elliptical intensity profile for the Toshiba visible laser diode and a comparison of generalized Lorentzian and Gaussian profiles. The laser diode electrical field distribution can cause problems with probe volume formation if proper corrective measures are not taken.

The diode electrical field is separable so the complete field is found simply by multiplying the two transverse profiles. The resulting optical field magnitude may then be represented by Eq. (4):

$$E(x, y) = \left[e^{(-4y^2/D_y^2)} \right] \left[\xi D_x^2 / \left(\xi D_x^2 + x^2 \right) \right] \tag{4}$$

For use in heterodyne LDA, the laser diode beam is split into two beams (A and B) each having equal electrical field magnitudes. Then the beams are focused to a crossing point where electromagnetic wave interference takes place.

The dimensions of the probe volume were found to be similar to those generated by Gaussian lasers with the exception that the beam dimension is no longer unique but rather has two distinct values $(d_{0x} \neq d_{0y})$. Equations (5–7) relate the input beam characteristics to the probe volume size:

$$l = 4\lambda f / \pi d_{0x} \tan(\Theta/2) \tag{5}$$

$$w = 4\lambda f / \pi d_{0x} \tag{6}$$

$$h = 4\lambda f / \pi d_{0y} \tag{7}$$

The probe volume fringes will not be as clean as those produced with a Gaussian laser beam. This phenomenon was investigated by Durst et al.[6] Essentially, the wave front curvature associated with the Lorentzian/Gaussian profile is greater than the curvature associated with a Gaussian profile. Near the crossing point the Lorentzian beam's phase does not reach the same level of uniformity as a Gaussian beam would. Consequently, the effects of beam divergence are heightened. Beam divergence in the crossing region will cause interference fringe planes to have curvature. Essentially, the fringe spacing seen by particles traveling in the x direction varies in the z and y directions. The effect is strongest when the beams are crossed with the Lorentzian distribution in the crossing plane.

In a laser diode generated probe volume, the fringe spacing increases as one moves toward the ends of the probe volume. Deviations can be as severe as $+10\%$ for Lorentzian beams (as opposed to roughly $+1\%$ for Gaussian). Accurate turbulence measurements are not possible without correcting for such high deviations. Actual fluid flow fluctuations (real turbulence) will be contaminated with fluctuations due to particle passing location (generating artificial turbulence). Durst et al.[6] showed that the artificial turbulence could
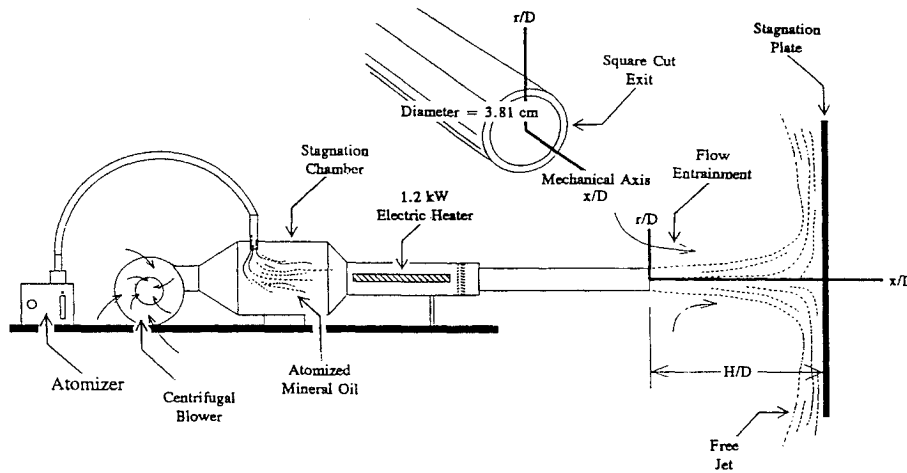
Fig. 5   Experimental test flow rig, turbulent, heated, stagnating, air jet.

be reduced by using frequency domain processing or by crossing the beams with the Gaussian profile in the crossing plane.

III.   Experimental Evaluation

With the miniature laser Doppler anemometer fully constructed and operational on an optical bread board, a quantification of the measurement uncertainty was required. A test flow was needed which would challenge the miniature LDA system. It was expected that the specific flow chosen would expose many of the LDA error sources, thereby enabling a systematic evaluation of the system's performance under realistic conditions.

Velocity measurements in a turbulent, stagnating, round jet ($Re = 33{,}600$) were chosen for the purpose of quantitative evaluation. The flow would have several attributes which would require special attention for accurate LDA measurements. Namely, the flow possessed large velocity gradients, high-local turbulence, large-scale intermittency, and a large mean velocity range. Figure 5 displays a schematic of the test flow facility.

Measurement surveys were performed at four x/D locations with three measurement devices: solid-state LDA, five-hole probe, and a single sensor hot-wire probe. The LDA data were computed based on 2000 individual Doppler bursts at 40 measurement points in the radial direction for each x/D location. Mineral oil of $1–3$-μm diameter was generated with a TSI six-jet atomizer and mixed with the air flow to be used as seed. The seeding density was set sufficiently low so that at most only one particle would be in the probe volume at a time. Uniform seed density was established through a seed containment tent which provided the entrained air with ample seed. Velocity measurements for the LDA data were computed via a TSI 1980B burst counter/processor interfaced to a personal computer.

IV.   Error Quantification for Fluid Dynamic Measurements

General Uncertainty Analysis Overview

The raw data measured with the laser diode-based miniature laser Doppler anemometer were put through a rigorous error analysis. It was desired to both correct for quantifiable bias errors and to compute measurement uncertainties based on estimates for uncorrectable error sources. The corrected mean velocity ($\bar{U}$) and rms turbulent velocity (u_{rms}) profiles with known uncertainties would then be compared to the hot-wire and five-hole probe data. It must be remembered that solid-state LDA probe volumes are different and would not necessarily have similar corrections to standard LDA systems.

Standard Uncertainty Analysis

The adopted standard measurement uncertainty methodology[7] was used exclusively in the analysis of the raw LDA data. The method provided a structured procedure for computing LDA measurement uncertainties based on the precision and bias errors of numerous sources.

The uncertainty of any single measurement or parameter can be expressed in terms of precision errors and bias errors. The estimated mean of the measurement may be assumed to be the average of N measurements (X_i). The bias error (B_X) is the shift in the measurement average from the true value. Because the true value is never exactly known, it is difficult to assign accurate values to bias error terms. The precision error is related to scatter of the measurement data. A value known as the precision index (S_X) is used to quantify the precision error. Equation (8) defines the precision index:

$$S_X = \sqrt{\sum_{i=1}^{N}(X_i - \bar{X})^2/(N-1)} \tag{8}$$

The errors in a particular result are directly related (through sensitivity factors) to the errors in the individual measurement parameters used to compute the result. A result such as

$$r = f\{P_i, P_{i+1}, P_{i+2} \ldots, P_j\} \tag{9}$$

is a function of j parameters, and the sensitivity factors are simply the derivatives of the result with respect to the parameters. Namely,

$$\theta_{P_i} = \frac{\partial r}{\partial P_i} \tag{10}$$

Each of the j measurement parameters will, in general, have a precision index (S_{P_i}) and a bias error (B_{P_i}) associated with it. The precision and bias errors in the result (S_r and B_r) due to the precision and bias in the parameters (S_{P_i} and B_{P_i}) is given by Eqs. (11) and (12):

$$S_r = \sqrt{\sum_{i=1}^{j}\left(\theta_{P_i} S_{P_i}\right)^2} \tag{11}$$

$$B_r = \sqrt{\sum_{i=1}^{j}\left(\theta_{P_i} B_{P_i}\right)^2} \tag{12}$$

If the parameters which are results themselves are used with other similarly computed parameters to compute a mean parameter (such as $\bar{U}$ from u_i, u_{i+1}, u_{i+3}, etc.), then the precision index and bias error in the mean value are given by

$$S_{\bar{X}} = t S_{X_i}/\sqrt{N} \tag{13}$$

$$B_{\bar{X}} = B_{X_i} \tag{14}$$

where N is the number of times the parameter X_i was independently determined and t is the student t value ($t \approx 2$ for $N \geq 30$). The

averaging process used to compute the result will tend to minimize the precision error, but the bias error will be unaffected.

The precision index and bias error in the rms value (such as u_{rms} from u_i, u_{i+1}, u_{i+2}, etc.) based on the precision and bias errors of a representative measurement are given by

$$S_{X_{rms}} = \frac{t(X_{rms})}{\sqrt{N}}\sqrt{\left[\frac{S_{X_i}}{X_{rms}}\right]^2 + \left[\frac{S_{\bar{X}}}{X_{rms}}\right]^2} \qquad (15)$$

$$B_{X_{rms}} = X_{rms} - \sqrt{(X_{rms})^2 - (S_{X_i})^2} \qquad (16)$$

The bias errors in individual measurements will have no effect on the uncertainty in the rms value. Bias errors will only shift the measurement distribution, but the data scatter will remain unchanged. However, the precision errors in the individual measurements will have a strong effect on the uncertainty in the rms value by broadening the measurement distribution.

The uncertainty in a result is taken to be a combination of both the precision and bias errors. For an uncertainty analogous to a 95% coverage, an rms combination was used:

$$U_r = \sqrt{B_r^2 + S_r^2} \qquad (17)$$

Miniature Laser Doppler Anemometer Uncertainty Sources

There were eight error sources investigated in the miniature LDA measurement uncertainty. Each of the error sources could potentially add both precision and bias errors to the computed mean velocity ($\bar{U}$) and the computed rms turbulent velocity (u_{rms}). An individual velocity measurement was calculated according to Eq. (18):

$$u_i = F_D \lambda/2 \sin(\Theta/2) \qquad (18)$$

The velocity calculation is seen to be a function of three parameters: Doppler frequency F_D, laser wavelength λ, and the crossing angle θ. Table 2 lists the error sources, the affected parameter, and the type of error incurred by each. In addition seed biasing was investigated to insure uniformity, but not quantified.

Two styles of error sources exist. Those which act on individual parameters and those which act on resultant calculations. The quantifiable error sources acting on $\bar{U}$ and u_{rms} were corrected for through appropriate relations. In contrast, the parameter error sources are coupled so they may not be accurately corrected for. Instead these errors were propagated into a resultant error to define a value of measurement uncertainty. The overall precision index and bias error in a single velocity measurement (Doppler burst) was computed as described previously by propagating the individual parameter errors into the instantaneous velocity result. Then the precision index and bias error for the 2000 individual velocity results were propagated again into the mean velocity and rms turbulent velocity results. Following the double propagation procedure, an uncertainty value was assigned to the mean velocity and the rms turbulence velocity through an rms combination of the respective precision index and bias error. This procedure was repeated for all 40 points in four separate profiles.

Table 2   Miniature LDA uncertainty error sources for individual
Doppler burst realization

Error source (effected parameter)	Errors on U_i
Crossing angle ($\theta/2$)	Bias only
Laser diode wavelength (λ)	Bias only
Interference plane gradients due to beam waist misalignments (F_D)	Precision and bias
Interference plane gradients due to Lorentzian intensity distribution (F_D)	Precision and bias
Signal processor comparison criteria and finite clock resolution	Precision only
High velocity biasing	Quantifiable mean velocity error
Velocity gradients across the finite probe volumn	Quantifiable rms turbulence error

Following the uncertainty procedure outlined, the resultant precision index and bias error in an instantaneous velocity measurement were found to be given by

$$S_{u_i} = \sqrt{\left(\frac{\partial u_i}{\partial F_D}S_{F_D}\right)^2 + \left(\frac{\partial u_i}{\partial \lambda}S_\lambda\right)^2 + \left(\frac{\partial u_i}{\partial(\Theta/2)}S_{\Theta/2}\right)^2} \qquad (19)$$

$$B_{u_i} = \sqrt{\left(\frac{\partial u_i}{\partial F_D}B_{F_D}\right)^2 + \left(\frac{\partial u_i}{\partial \lambda}B_\lambda\right)^2 + \left(\frac{\partial u_i}{\partial(\Theta/2)}B_{\Theta/2}\right)^2} \qquad (20)$$

where the precision index for F_D is a combination of four precision indices as shown in Eq. (21):

$$S_{F_D} = \sqrt{\left(S_{F_{D1}}\right)^2 + \left(S_{F_{D2}}\right)^2 + \left(S_{F_{D3}}\right)^2 + \left(S_{F_{D4}}\right)^2} \qquad (21)$$

Crossing Angle Measurement Uncertainty

Because of the experimental method used for measuring the half-angle, a bias error existed. Laser diode beam propagation vectors (in three dimensions) were determined with the aid of a pinhole and a precision 3-axis traverse. The angle between the two beams was then found by using the dot product relation between the two spatial vectors. The beam crossing angle should not change in time (neglecting laser beam walk which is small for laser diodes) so every seed particle would see a probe volume defined by the same crossing angle ($S_{\theta/2} = 0$ rad). The current measurement capabilities allowed a bias error of 0.01 deg ($B_{\theta/2} = 1.75 \times 10^{-4}$ rad) for the half-angle measurement.

Laser Diode Wavelength Uncertainty

The laser diode wavelength was not known exactly due to junction temperature drift resulting in a bias error. In general, the wavelength emitted by the laser diode was a function of junction temperature, forward bias current, and reflected laser light. The laser diode was driven with a highly stable constant current source, and the LDA system used only high-quality optics with antireflective coatings. However, the temperature of the junction was not actively controlled. Consequently, the laser diode wavelength was able to drift from the value measured at the beginning of the measurements to that at the end ($\sim$1 h). However, it was assumed that the temperature remained constant during a single velocity computation comprised of 2000 Doppler bursts ($S_\lambda = 0$ nm). This results in a bias error for each individual velocity computation. The bias error B_λ was found to be 0.5 nm for temperature fluctuations of $\pm 2°C$.

Interference Plane Gradients due to Misalignments

Because of misalignments of the laser beam waist, the spacing between interference fringes may not be uniform throughout the probe volume causing a precision error. Hanson[8] describes in detail the source of interference plane gradients. Essentially, a misplacement of the input beam waist causes a spatial difference between the beams crossing point and the location of minimum beam diameters. This spatial gap forces the probe volume to be formed by laser beams that are diverging. Such a situation causes the interference fringes to fan out having a different spacing at either end of the probe volume. Following Hanson,[8] the precision index $S_{F_{D1}}$ was computed to be $(1.69 \times 10^{-3})F_D$. The bias error from such a source is small and was neglected ($B_{F_{D1}} = 0$).

Interference Plane Gradients due to Lorentzian Distribution

Because of the Lorentzian intensity distribution in the plane of the beam crossing (x–z plane), the interference planes will be distorted additionally from those due to misalignments. The Lorentzian distribution error was discussed in detail by Durst et al.[6] The cause of the error stems from the high wave front curvature and unevenness present with Lorentzian diode beams. Even for a properly aligned LDA system, the high wave front curvature will cause the interference fringes to be curved. The fringe curvature becomes worse as the ends (along length) of the probe volume are approached. Following Durst et al.,[6] the precision index $S_{F_{D2}}$ and bias error $B_{F_{D2}}$ were estimated to be 0.065 and 0.01 times the Doppler frequency, respectively.

Signal Processor Comparison Criteria and Finite Clock Resolution

The signal processor due to its comparison criteria and finite clock resolution was not able to report the captured Doppler frequency with zero uncertainty. Errors due to amplifier noise, filter settings, and false triggering were encompassed into the comparison error. A comparison criteria of 1% was used for validating the processing of an individual Doppler burst, and the processor clock had a resolution of 1 ns. For timing eight cycles the two precision indices became $(0.01)F_D$ for the comparison criteria $S_{F_D 3}$ and $(1.25 \times 10^{-10} \text{ s})F_D^2$ for the clock resolution $S_{F_D 4}$.

High-Velocity Biasing

High-velocity biasing results from the method with which Doppler bursts are collected via time domain processing (counter processors). The subject of high-velocity biasing was treated by McLaughlin and Tiederman.[9] If the flow under study is uniformly seeded, then there is a higher than average mass flow of seed when the instantaneous velocity is greater than the mean velocity. Similarly, when the instantaneous velocity is below the mean velocity, there is a less than average mass flow of seed. As a result, there is a higher probability for a Doppler burst to be generated under high-velocity conditions than under low-velocity conditions. This biasing tends to cause the measured mean velocity $\bar{U}$ to be too high and the measured rms turbulent velocity u_{rms} to be too low.

It was decided to apply the one-dimensional correction scheme suggested by McLaughlin and Tiederman[9] for the current research. This scheme assumes an ellipsoidal probe volume generating one-dimensional measurements. Clearly, the aforementioned probe volume assumption would be expected to cause minor errors in the bias corrections due to the different laser diode probe volume.

From McLaughlin and Tiederman,[9] the following functional relationships were derived to correct the measured mean velocity $\bar{U}$:

$$\frac{\bar{U}_{\text{measured}}}{\bar{U}_{\text{corrected}}} - 1 \simeq 0.0599 \left(\frac{u_{rms}}{\bar{U}}\right)_{\text{measured}} + 0.7445 \left(\frac{u_{rms}}{\bar{U}}\right)^2_{\text{measured}}$$

(22)

and the measured rms turbulent velocity (u_{rms}):

$$\left(\left(\frac{u_{rms}}{\bar{U}}\right)_{\text{measured}} \middle/ \left(\frac{u_{rms}}{\bar{U}}\right)_{\text{corrected}}\right) - 1$$

$$\simeq 0.0349 \left(\frac{u_{rms}}{\bar{U}}\right)_{\text{measured}} - 1.2361 \left(\frac{u_{rms}}{\bar{U}}\right)^2_{\text{measured}}$$

(23)

Velocity Gradients Across the Finite Probe Volume

Finite spatial resolution biasing results from the presence of mean velocity gradients across the probe volume dimensions. When a mean velocity gradient exists across the probe volume, the resulting Doppler bursts from different individual particles will have different frequencies in different regions of the probe volume. Consequently, even in a laminar flow with velocity gradients, the LDA system would measure turbulence due to the varying mean velocities across the probe volume.

Some simplifying assumptions allow corrections for one-dimensional LDA systems. The velocity gradients may be assumed linear throughout. In addition, the probe volume length is typically much longer than its width or height so that gradients only along the length are significant. For such a situation the mean velocity $\bar{U}$ will not be affected, but the measured rms turbulent velocity u_{rms} will be reported too high.

A numerical study of the expected bias error was done. A theoretical probe volume was seeded with 10,000 particles in a simulated laminar flow. The velocity gradient was placed along the probe volume length z axis. The probability of a measurement occurring at a specific location in the probe volume was assumed to be Gaussian. The actual probability distribution, as with high-velocity biasing, was not known, and this uncertainty would of course lead to minor errors. The Gaussian distribution was truncated at the $1/e^2$ points on
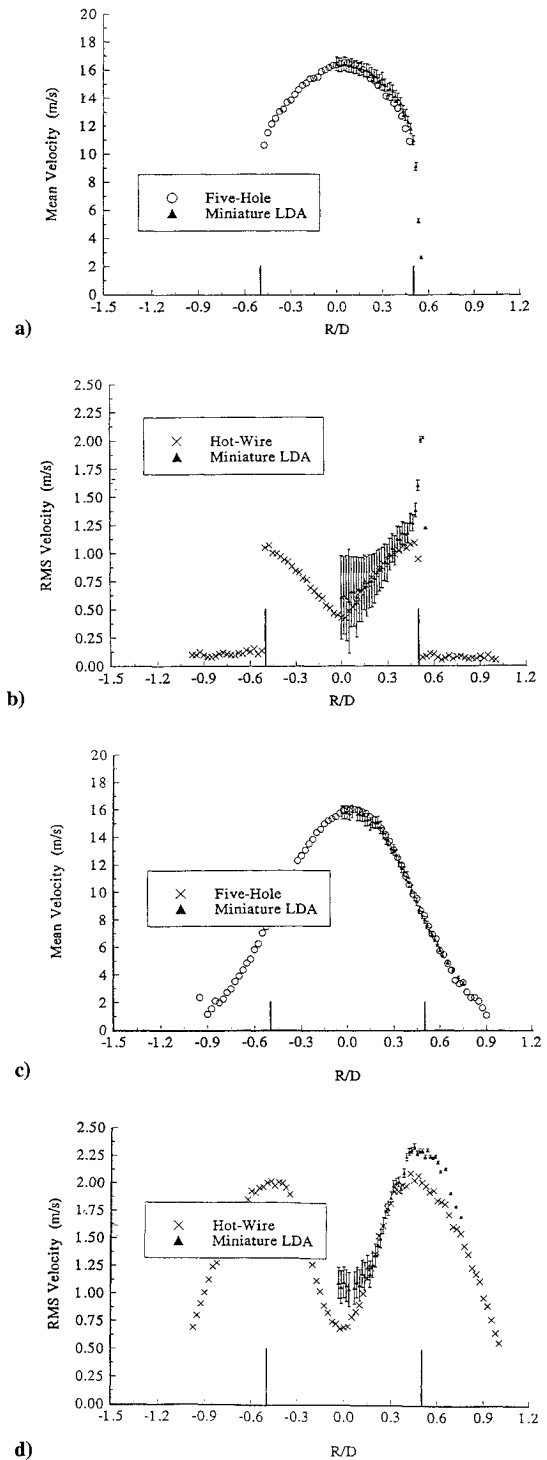
Fig. 6 Stagnating jet corrected profile with uncertainty bands for $H/D = 8$: a) $x/D = 0$ profile mean velocity, b) $x/D = 0$ profile rms, turbulent velocity, c) $x/D = 4$ profile mean velocity, and d) $x/D = 4$ profile rms, turbulent velocity.

both the high and low ends. The resultant effect of the velocity gradient was to report an additional rms turbulent velocity as given by

$$(u_{rms})_{\text{additional}} \simeq (1.0 \times 10^{-4}) \frac{d\bar{U}}{dz}$$

(24)

Experimental Results Following Corrections and Uncertainty

The raw miniature LDA measurement results were put through the uncertainty procedure described thus far. The measurements were corrected for expected bias errors due to both high-velocity biasing and finite spatial-resolution biasing. Then uncertainties were determined for the corrected measurements based on errors in
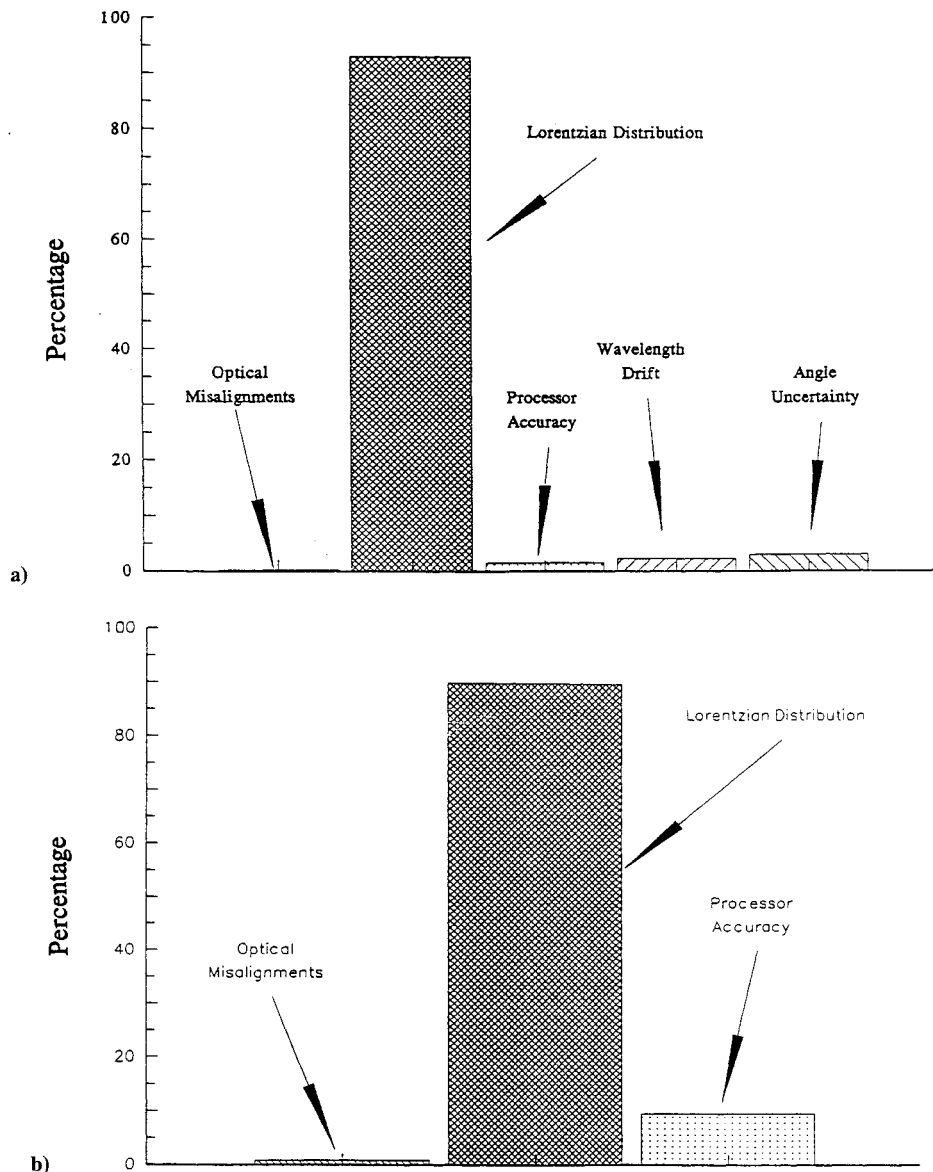
Fig. 7   Relative weighting of uncertainty sources for a) mean velocity and b) rms, turbulent velocity.

half-angle measurement, laser diode wavelength uncertainty, interference plane gradients (due to misalignments and Lorentzian distribution), and signal processor resolution. Figure 6 displays measured profiles for $x/D = 0$, and $x/D = 4$ following bias corrections and uncertainty calculations. Comparisons between LDA, five-hole probe, and hot-wire were quite good. Although the comparisons would not be exact even given perfect instruments (LDA is one dimentional whereas hot-wire and five-hole have three-dimensional effects) much can be observed from such a comparison.

Relative Weighting of Uncertainty Errors

It is interesting to examine the relative weighting of the uncertainty errors with respect to the mean velocity U and the rms turbulent velocity u_{rms}. Figure 7 displays a bar graph showing the relative weighting of the six uncertainty sources on the mean velocity and rms turbulence measurements.

V.   Conclusions

The performance of a visible index guided laser diode in a miniature LDA system was evaluated. Error quantification for both laser diode and fluid dynamic related quantities was performed.

Laser diode technology was researched in an effort to reveal any possible complications with their use in an LDA system. Many problems were uncovered including high beam divergence,

high astigmatism, low coherence, multiple simultaneously emitted modes, elliptic beam profile, non-Gaussian intensity profile, and wavelength instabilities. Effective corrective measures were needed to counter each of the individual problems.

A thorough quantitative analysis was performed using experimental measurements. A stagnating round jet ($Re = 33,600$) was traversed with the miniature LDA ($\bar{U}$ and u_{rms}), a five-hole probe ($\bar{U}$), and a single sensor hot-wire probe (u_{rms}). Following corrections for correctable LDA bias errors, measurement uncertainties were computed. The corrected measurements were compared to five-hole probe and hot-wire measurements. The miniature LDA was found to correlate very well with the two other probe styles. For the present LDA configuration the mean velocity measurements compared within 2% of five-hole probe data, and the rms turbulent velocity measurements compared within 5–20% of hot-wire probe data. In most cases the predicted uncertainty was large enough to explain the measurement error observed. The main source of uncertainty was found to be associated with the Lorentzian distribution in the crossing plane (x–z plane).

It is believed that solid-state LDA systems have a promising future in the field of laser Doppler anemometry. Their potential advantages will make them a plausible choice over fiber-optic-based LDA systems. Presently, high-quality single component LDA systems can be constructed, and their applicability is only restricted by their moderate powers and limited wavelength availability. It is expected

that visible laser diode choices, now somewhat limited, will expand greatly in the future. Already quality, visible laser diode optical powers are at the 30–50-mW level in various wavelengths. It is recommended that future systems be constructed with the Gaussian profile in the crossing plane (x–z plane). This can easily be accomplished by rotating the laser diode 90 deg and using appropriate 1/2 retarder wave plates for polarization control. Laser diode astigmatisms are getting lower, and the elliptical, non-Gaussian electric field is receiving attention from research in the telecommunications field.

References

[1]Bopp, S., Durst, F., Müller, R., Naqwi, A., Tropea, C., and Weber, H., "Small Laser-Doppler Anemometers Using Semiconductor Lasers and Avalanche Photodiodes," *Applications of Laser Anemometry to Fluid Mechanics*, 4th International Symposium, Springer–Verlag, Berlin, 1988, pp. 313–329.

[2]Damp, S., "Battery-Driven Miniature LDA-System With Semiconductor Laser Diode," *Applications of Laser Anemometry to Fluid Mechanics*, Fourth International Symposium, Springer–Verlag, 1988, pp. 338–360.

[3]Durst, F., and Stevenson, W. H., "Influence of Gaussian Beam Properties on Laser Doppler Signals," *Applied Optics*, Vol. 18, No. 4, 1979, pp. 516–524.

[4]Mackenzie, M. R., Tieu, A. K., Kosasih, P. B., and Binh, L. N., "A Visible Wavelength Solid-State LDA and Application to Thin Channel Flow," *Measurement Science and Technology*, IOP Publishing Inc., UK, Vol. 3, 1992, pp. 852–857.

[5]McLean, C., and Camci, C., "Miniature Laser Doppler Anemometers Using Solid-State Laser Diodes," *International Symposia on Lasers, Sensors, Applications*, Session Solid-State Lasers IV, Vol. 1864, Society of Photo-Optical Instrumentation Engineers, 1993, pp. 163–179.

[6]Durst, F., Müller, R., and Naqwi, A., "Semiconductor Laser Doppler Anemometer for Applications in Aerodynamic Research," *AIAA Journal*, Vol. 30, No. 4, 1991, pp. 1033–1038.

[7]Abernethy, R. B., Benedict, R. P., and Dowdell, R. B., "ASME Measurement Uncertainty," *Journal of Fluids Engineering*, Vol. 107, June 1985, pp. 161–164.

[8]Hanson, S., "Broadening of the Measured Frequency Spectrum in a Differential Laser Anemometer Due to Interference Plane Gradients," *Journal of Physics D: Applied Physics*, Vol. 6, 1973, pp. 164–171.

[9]McLaughlin, D. K., and Tiederman, W. G., "Biasing Correction for Individual Realization of Laser Anemometer Measurements in Turbulent Flows," *Physics of Fluids*, Vol. 16, No. 12, 1973, pp. 2082–2088.